Eur. Phys. J. B **53**, 387–394 (2006)
DOI: 10.1140/epjb/e2006-00394-3

THE EUROPEAN PHYSICAL JOURNAL B

S-matrix pole trajectories in quantum wires with resonantly coupled cavities

G. Cattapan[1,2,a], P. Lotti[2,1], and A. Pascolini[1,2]

[1] Dipartimento di Fisica "G. Galilei", Università di Padova, via F. Marzolo 8, 35131 Padova, Italy
[2] Istituto Nazionale di Fisica Nucleare, Sezione di Padova, via F. Marzolo 8, 35131 Padova, Italy

Received 1st June 2006 / Received in final form 20 September 2006
Published online 27 October 2006 –

Abstract. We consider a T-shaped, one-dimensional quantum waveguide containing an attractive or repulsive impurity in the lateral stub, and study how the resonance poles move in the complex k-plane when the strength or the position of the defect changes. Similarities and differences with respect to standard potential scattering problems are highlighted.

PACS. 73.63.Nm Quantum wires – 73.23.Ad Ballistic transport – 72.10.Fk Scattering by point defects, dislocations, surfaces, and other imperfections (including Kondo effect)

1 Introduction

Electronic transport in ultra-small semiconductor structures has inspired a lot of experimental and theoretical work in the last several years [1,2]. In high-purity materials and at low temperatures, the electron's motion is ballistic, and gives rise to quantum interference effects, which can be studied as a quantum transmission problem [2,3]. It has been found that mesoscopic devices may exhibit sharp transmission minima, which can be interpreted as resonance phenomena, with a Fano-type line shape. In particular, two–dimensional quantum wave guides coupled to a T-stub resonator have attracted considerable attention (see, for instance, references [4–7] and references quoted therein). Much as in atomic physics, the Fano resonances occurring in the transmission coefficient of quantum wires can be interpreted as due to the coupling of a quasi-bound-state with a continuum of states.

Electron's transport in two-dimensional structures, and the occurrence and features of Fano resonances have been investigated both theoretically and numerically in the past several years employing different techniques, ranging from the Green's function [4,8–10] to the transfer [5] and scattering matrix [11,12] approach. While these 2D models have reached by now a considerable level of sophistication, useful insights can be still obtained through simple, one-dimensional calculations, when the transverse dimension of the wire is small enough. In such a case, indeed, the electron's motion in the transverse direction is confined in the lowest-energy subband, and one can limit oneself to consider the electron's dynamics in the propagation direction only. Fano resonances in one-dimensional quantum waveguides coupled to a stub have been considered by Shao et al. several years ago [13,14]. By studying the scattering amplitude for these systems in the complex energy plane, they have been able to show that the resonances are associated to zero-pole pairs, which lead to sharp variations of the transmission coefficient with energy.

In references [13,14] the location of the resonance poles has been determined for an empty stub, or for a stub coupled weakly to the principal wire, because of the presence of a repulsive barrier at the point where the wire and the sidearm join together. As a natural extension of this analysis, one can study how the pole location of the scattering matrix and the transmission properties of the device are affected by a change in the strength or the position of a potential field inside the stub. A quasi-one-dimensional system of this type represents a schematic model of a stubbed quantum wave guide, in presence of a defect or of an external bias in the attached cavity.

From a more general point of view, the above analysis of the scattering operator for a stubbed wave guide can be regarded as the extension to quasi-one-dimensional systems of well-known results of standard potential scattering theory [15,16]. For finite-range potentials, or potentials decreasing at infinity faster than any exponential, one has exhaustive information about the location of the S-matrix poles in the complex energy or momentum

[a] e-mail: giorgio.cattapan@pd.infn.it

plane [16,17]. In particular, a by now text-book example is provided by s-wave scattering by a spherical potential well [15,16]. As the strength of the interaction becomes more and more negative, the poles of the S-matrix move in pairs in the fourth and third quadrant of the momentum plane, emerging with an infinite imaginary part, until each pair coalesces on the negative imaginary axis, to originate a double pole. Beyond this point, one has an anti-bound state pole moving downward and a pole moving upward on the imaginary axis; the latter reaches finally the positive imaginary axis, to become a pole associated to a new bound state of the interaction. In our opinion, it is worth to ascertain to what extent these features of the scattering operator survive when the interaction acts inside a quasi-one-dimensional system.

We evaluate the scattering operator for the stubbed wave guide in correspondence to a realistic, smooth potential in the sidearm. To this end, we approximate the potential by a series of square wells or barriers, depending upon the sign of the strength, and write the total transfer matrix for the stub as the product of partial transfer matrices, which can be expressed in simple, analytic form. The poles of the device S-matrix occur in correspondence to the zeros of a simple function of the stub transfer matrix. We determine numerically these zeros, thereby getting the pole trajectories in the complex momentum plane as the strength or the position of the defect potential changes. Thus, our numerical experiments allow one to get insight into the response of the system to changes in its dynamical or geometrical features; at the same time, one can exhibit similarities and differences between a scattering problem defined on a quasi-one-dimensional system, and what happens in standard potential scattering theory.

The formalism needed to get the total S-matrix is outlined in Section 2. The outcome of our calculations is presented in Section 3, while a brief summary of our results and conclusions are given in Section 4.

2 Evaluation of the scattering matrix

We shall consider the T-stub structure shown in the inset of Figure 1. It consists of an infinitely long, straight perfect wire, with a dangling sidearm of length L. The sidearm may contain a defect, described by a model potential, located in the region $l_1 \leq y \leq l_2$. If the wires are thin enough, one can describe the device through a simple one–dimensional model. The wave function in the principal wire can then be written as a superposition of incoming and outgoing plane waves. On the left of the branch point one has

$$\psi_L(x) = \overrightarrow{c}_L e^{ikx} + \overleftarrow{c}_L e^{-ikx}, \tag{1a}$$

where the wave number k is related to the electron's energy E and effective mass m^* by the usual relation $k = \sqrt{2m^*E}/\hbar$. Similarly, on the right of the branch point

$$\psi_R(x) = \overrightarrow{c}_R e^{ikx} + \overleftarrow{c}_R e^{-ikx}. \tag{1b}$$

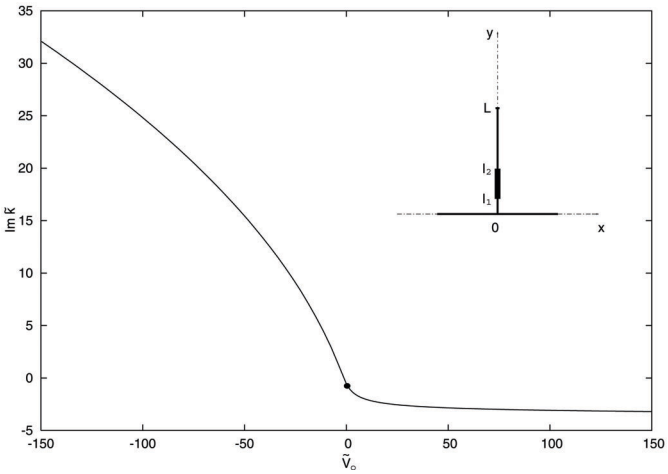

Fig. 1. Position of the $n = 0$ pole on the imaginary axis for $-150 \leq \tilde{V}_0 \leq 150$. The potential $f(\tilde{y})$ is a double Woods-Saxon with geometric parameters $\tilde{l}_1 = 0.1$, $\tilde{l}_2 = 0.3$, and $\tilde{a} = 5\times10^{-3}$. The dot marks the pole position in the unperturbed case $\tilde{V}_0 = 0$. The inset gives a schematic picture of the considered T-stub device, having a sidearm of length L with a defect between $y = l_1$ and $y = l_2$.

We shall assume that the defect potential becomes vanishingly small outside the region $l_1 \leq y \leq l_2$, so that one has incoming and outgoing plane waves for $0 \leq y \leq l_1$, and $l_2 \leq y \leq L$, whereas there will be distorted waves in the region where the potential acts, namely

$$\psi_{S_1}(y) = c^{\uparrow}_{S_1} e^{iky} + c^{\downarrow}_{S_1} e^{-iky} \qquad 0 \leq y \leq l_1, \tag{2a}$$

$$\psi_D(y) = c^{\uparrow}_D \varphi(y) + c^{\downarrow}_D \phi(y) \qquad l_1 \leq y \leq l_2, \tag{2b}$$

$$\psi_{S_2}(y) = c^{\uparrow}_{S_2} e^{iky} + c^{\downarrow}_{S_2} e^{-iky} \qquad l_2 \leq y \leq L. \tag{2c}$$

The wave functions in the main wire and in the stub have to match smoothly at the junction. The continuity of the solution of the Schrödinger equation requires that

$$\psi_L(x=0) = \psi_{S_1}(y=0) = \psi_R(x=0), \tag{3}$$

while current conservation can be guaranteed provided that the derivatives of the wave functions satisfy the condition [18,19]

$$\psi'_L(x=0) = \psi'_{S_1}(y=0) + \psi'_R(x=0). \tag{4}$$

A straightforward calculation yields the linear relations

$$\overrightarrow{c}_L + \overleftarrow{c}_L = c^{\uparrow}_{S_1} + c^{\downarrow}_{S_1}, \tag{5a}$$

$$\overrightarrow{c}_R + \overleftarrow{c}_R = c^{\uparrow}_{S_1} + c^{\downarrow}_{S_1}, \tag{5b}$$

and

$$\overrightarrow{c}_L - \overleftarrow{c}_L = c^{\uparrow}_{S_1} - c^{\downarrow}_{S_1} + \overrightarrow{c}_R - \overleftarrow{c}_R, \tag{5c}$$

among the ingoing and outgoing amplitudes.

Equations (5) have to be supplemented with matching conditions at $y = l_1$ and $y = l_2$ between the wave functions

$\psi_{S_1}(y)$, $\psi_D(y)$, and $\psi_{S_2}(y)$, together with the condition that $\psi_{S_2}(y)$ vanishes at $y = L$. The latter requirement implies

$$c^{\uparrow}_{S_2} = -e^{-2ikL} c^{\downarrow}_{S_2}, \tag{6}$$

while, equating the logarithmic derivatives at $y = l_1$ and $y = l_2$ one has

$$\begin{pmatrix} c^{\uparrow}_{S_1} \\ c^{\downarrow}_{S_1} \end{pmatrix} = \begin{pmatrix} M_{11}^{(S_1|D)} & M_{12}^{(S_1|D)} \\ M_{21}^{(S_1|D)} & M_{22}^{(S_1|D)} \end{pmatrix} \begin{pmatrix} c^{\uparrow}_{D} \\ c^{\downarrow}_{D} \end{pmatrix}, \tag{7a}$$

$$\begin{pmatrix} c^{\uparrow}_{D} \\ c^{\downarrow}_{D} \end{pmatrix} = \begin{pmatrix} M_{11}^{(D|S_2)} & M_{12}^{(D|S_2)} \\ M_{21}^{(D|S_2)} & M_{22}^{(D|S_2)} \end{pmatrix} \begin{pmatrix} c^{\uparrow}_{S_2} \\ c^{\downarrow}_{S_2} \end{pmatrix}, \tag{7b}$$

where the matrices $\mathbf{M}^{(S_1|D)}$ and $\mathbf{M}^{(D|S_2)}$ are defined according to

$$M_{j1}^{(S_1|D)} \equiv \tfrac{1}{2}\left[\varphi(l_1) - (-1)^j \tfrac{1}{ik}\varphi'(l_1)\right] e^{(-1)^j ikl_1}, \tag{8a}$$

$$M_{j2}^{(S_1|D)} \equiv \tfrac{1}{2}\left[\phi(l_1) - (-1)^j \tfrac{1}{ik}\phi'(l_1)\right] e^{(-1)^j ikl_1}, \tag{8b}$$

and

$$M_{1j}^{(D|S_2)} \equiv \frac{(-1)^{j-1} ik\phi(l_2) - \phi'(l_2)}{2W(\phi\,,\varphi)} e^{(-1)^{j-1} ikl_2}, \tag{9a}$$

$$M_{2j}^{(D|S_2)} \equiv \frac{\varphi'(l_2) + (-1)^j ik\varphi(l_2)}{2W(\phi\,,\varphi)} e^{(-1)^{j-1} ikl_2}, \tag{9b}$$

with $j = 1,\ 2$. Here, $W(\phi, \varphi) \equiv \phi\varphi' - \varphi\phi'$ denotes the Wronskian of the two linearly independent solutions $\phi(y)$ and $\varphi(y)$, *i.e*, of the incoming and outgoing wave functions in the defect region. The operators $\mathbf{M}^{(S_1|D)}$ and $\mathbf{M}^{(D|S_2)}$ represent the partial transfer matrices between the empty regions and the region occupied by the defect in the stub.

Equations (7a) and (7b) can be combined together to express the amplitudes $c^{\uparrow}_{S_1}$ and $c^{\downarrow}_{S_1}$ linearly in terms of the pair $c^{\uparrow}_{S_2}$, $c^{\downarrow}_{S_2}$ through the stub transfer matrix

$$\mathbf{M}^{(s)} = \mathbf{M}^{(S_1|D)} \mathbf{M}^{(D|S_2)}. \tag{10}$$

Using equation (6) to write the wave amplitudes at the junction as functions of $c^{\uparrow}_{S_2}$, and solving the matching conditions (5a), (5b), and (5c) with respect to the outgoing waves $\overleftarrow{c}_L$ and $\overrightarrow{c}_R$ one finally gets the total scattering operator $\mathbf{S}$ for the device, namely

$$\begin{pmatrix} \overleftarrow{c_L} \\ \overrightarrow{c_R} \end{pmatrix} = \begin{pmatrix} S_{11} & S_{12} \\ S_{21} & S_{22} \end{pmatrix} \begin{pmatrix} \overrightarrow{c_L} \\ \overleftarrow{c_R} \end{pmatrix}, \tag{11}$$

where

$$\begin{pmatrix} S_{11} & S_{12} \\ S_{21} & S_{22} \end{pmatrix} \equiv \begin{pmatrix} \frac{D_2 - D_1}{3D_1 + D_2} & \frac{2(D_1 + D_2)}{3D_1 + D_2} \\ \frac{2(D_1 + D_2)}{3D_1 + D_2} & \frac{D_2 - D_1}{3D_1 + D_2} \end{pmatrix}, \tag{12}$$

and the quantities D_1 and D_2 are given in terms of the stub transfer matrix by

$$D_j \equiv 2\left(M_{j2}^{(s)} - e^{-2ikL} M_{j1}^{(s)}\right), \qquad j = 1,\ 2. \tag{13}$$

The matrix elements S_{11} and S_{21} represent the reflection and transmission amplitudes, respectively, for an electron's wave impinging from the left on the stub, while S_{22} and S_{12} are the corresponding quantities for a wave incoming from the right [1,2]. Equation (12) exhibits the symmetry of the scattering operator ensuing from the time-reversal invariance of the system, and allows one to evaluate the transmission coefficient $T = |S_{21}|^2$ of the device, once the stub transfer matrix $\mathbf{M}^{(s)}$ is known. As for the latter, the non-trivial part of the calculation is the evaluation of the wave functions $\phi(y)$ and $\varphi(y)$.

For a generic potential $V(y) = V_0 f(y)$, a simple way to evaluate the stub M-matrix is provided by the "slicing" method [20]. One sub-divides the interval $[l_1,\ l_2]$ where $V(y)$ is not negligible into N sub-intervals, and evaluates the interaction at N points $y_n^{(c)}$ $(n = 1, \ldots, N)$, each being the midpoint of the corresponding sub-interval. The original interaction is thus replaced by a sequence of square barriers or wells, having effective strengths $V(n) \equiv V_0 f(y_n^{(c)})$, where the electron propagates in plane-wave states with wave number $q_n = \sqrt{2m^*\,(E - V(n))}/\hbar$. In these circumstances the transfer matrix $\mathbf{M}^{(n|n+1)}$ from the nth region to region $n + 1$ can be straightforwardly evaluated by matching the logarithmic derivatives at the boundary $y = y_n$, and written in simple, analytic terms as a function of the wave numbers q_n and q_{n+1} in the two regions. The total stub transfer matrix is finally obtained through the usual multiplication rule

$$\mathbf{M}^{(s)} = \prod_{n=0}^{N} \mathbf{M}^{(n|n+1)}, \tag{14}$$

where one has $y_0 = l_1$, $q_0 \equiv k$, and $y_N = l_2$, $q_{N+1} \equiv k$.

Finally, it is worth to add some considerations about the bound-state problem, and the analytical properties of the S-matrix. If the potential in the stub supports a bound state for $E < 0$, one has exponentially decaying waves spreading through the junction both on the left and on the right in the main wire. Replacing the real wave number k with $i\chi \equiv i\sqrt{2m^*|E|}/\hbar$ in equations (1), one recognizes that, to avoid diverging waves, one must set $\overrightarrow{c_L} = \overleftarrow{c_R} = 0$, namely one has to exclude incoming waves in the boundary conditions. One can then repeat the procedure followed for the scattering case, everything going through unchanged as far as the matching conditions are concerned, and one arrives at a secular equation which has a non trivial solution if and only if

$$(3D_1 + D_2) = 0. \tag{15}$$

Comparing equation (15) with equation (12), one has that, in correspondence to the possible bound states of the system, the analytic continuation of the scattering matrix has poles on the positive imaginary axis, in complete analogy with potential scattering theory.

Resonances of the T-stub device are associated to poles of the S-matrix in the fourth quadrant of the complex k-plane. Starting from equation (14), one can verify by

inspection that the stub transfer matrix satisfies the identity

$$M_{ij}^{(s)}(-k^*) = M_{ij}^{(s)}(k)^*, \tag{16}$$

where, as usual, A^* represents the complex conjugate of A. Because of equations (13), this property can be transferred immediately to the total scattering matrix, i.e.,

$$\mathbf{S}(-k^*) = \mathbf{S}(k)^*. \tag{17}$$

In other words, as in potential scattering theory, each pole of the S-matrix in the fourth quadrant has its mirror image in the third quadrant of the complex momentum plane.

3 Selected numerical examples

We have determined the location of the poles of the scattering matrix (12) in the complex momentum plane by looking for the zeros of the denominator $\mathcal{D} \equiv 3D_1 + D_2$ for a given position and strength of the potential in the sidearm. Since the shape of the transmission coefficient as a function of energy is essentially determined by the poles and by the zeros of S_{21} [13,14], we have also looked for the zeros of the numerator $\mathcal{N} \equiv 2(D_1 + D_2)$, which occur on the positive, real axis [14]. In both cases, the zeros have been found through various numerical methods, in order to check the reliability of the results, starting the search procedure from the corresponding empty-stub k-values. As a matter of fact, for $V_0 = 0$, the scattering matrix of the system can be given in a simple, analytic form, i.e. [14],

$$\mathbf{S} = \begin{pmatrix} \dfrac{e^{2ikL}+1}{e^{2ikL}-3} & 2\dfrac{e^{2ikL}-1}{e^{2ikL}-3} \\ 2\dfrac{e^{2ikL}-1}{e^{2ikL}-3} & \dfrac{e^{2ikL}+1}{e^{2ikL}-3} \end{pmatrix}. \tag{18}$$

It is an easy task to show that the poles of this S–matrix occur at $k_n^{(p)} = \dfrac{n\pi}{L} - \dfrac{i}{2L}\ln 3$ with $n = 0,\ \pm 1,\ \pm 2, \ldots$, whereas one has transmission zeros at $k_n^{(o)} = \dfrac{n\pi}{L}$. In particular, for positive n, one gets resonance poles in the fourth quadrant of the complex momentum plane.

Most of the results we shall present refer to a potential with a realistic, smooth profile of the Wood-Saxon (WS) type, i.e.,

$$V(y) = V_0 \begin{cases} 1 - \left[1 + e^{(y-y_{c_1})/a}\right]^{-1} & y \le \frac{y_{c_1}+y_{c_2}}{2}, \\ \left[1 + e^{(y-y_{c_2})/a}\right]^{-1} & y \ge \frac{y_{c_1}+y_{c_2}}{2}, \end{cases} \tag{19}$$

where c_1 and c_2 are the inflexion points of the profile function, so that the potential is centered at $y_c = (y_{c_1} + y_{c_2})/2$, and a plays the role of a diffuseness parameter. For $a \to 0$, the potential approaches a simple square well or barrier, according to the negative or positive sign of the strength parameter. For $a \neq 0$, we verified that good convergence is achieved with 10 slices.

To allow for the scaling of the problem to different stub dimensions, all lengths will be given in terms of L, wave numbers in terms of $1/L$, while energies will be expressed in units of $\epsilon_1 = \hbar^2\pi^2/2m^*L^2$, the ground-state energy of an infinitely deep well of width L. The diffuseness parameter has been chosen so as to guarantee that the potential is negligible outside the region $\tilde{l}_1 \le \tilde{y} \le \tilde{l}_2$, where symbols with a tilde refer to adimensional quantities; we assumed $\tilde{a} = 5 \times 10^{-3}$, which, for a stub 100 Å long, means $a = 0.5$ Å. Both the interaction (19) and square barriers or wells have been considered in our calculations; it turned out that the essential features of the pole trajectories do not change substantially in passing from a square to a smooth potential, an indication that the transmission coefficient of the device does not depend in an essential way upon the details of the potential profile.

In Figure 1 we give the trajectory of the pole with $n = 0$ for a double Woods-Saxon potential centered at $\tilde{y}_c = 0.2$, when the strength varies from $-150\ \epsilon_1$ up to $150\ \epsilon_1$. For positive, increasing strengths one observes an anti-bound state pole moving downward along the negative imaginary axis. The pole moves more and more slowly as $\tilde{V}_0$ increases, its position becoming insensitive to the value of the strength for $\tilde{V}_0 > 150$. This "saturation" effect in the pole's motion can be related to the wave function behavior in the stub. As a matter of fact, for high repulsive strengths, the wave function is strongly suppressed across the potential, and is practically independent of the potential strength.

For attractive strengths, the pole moves upward, starting from the unperturbed position, and passes into the physical ($\mathrm{Im}k > 0$) region of the imaginary axis, when $\tilde{V}_0 \simeq -1.34$. In such a situation, therefore, a first bound state can be supported by the potential in the resonator. For decreasing strengths, the bound-state pole moves upward along the positive imaginary axis, since the electron becomes more and more deeply bound, as it was to be expected.

In Figure 2 we exhibit the trajectory of the first pair of poles ($n = \pm 1$) with varying strength, for the same potential position as above. The two poles occur at symmetric positions with respect to the imaginary axis, as required by equation (17). For repulsive strengths ($0 \le \tilde{V}_0 \le 180$), the resonance pole moves toward the right, starting from the unperturbed position, and approaches the real axis; this corresponds to an increasing repulsive effect on the corresponding transmission resonance, which is shifted to higher and higher energies, while becoming narrower and narrower. The pole motion can be interpreted in the light of the behavior of the wave function in the sidearm, evaluated at the physical energy $\mathrm{Re}\tilde{E}^{(p)}$, where $\tilde{E}^{(p)} = (\tilde{k}^{(p)})^2/\pi^2$ is the pole position in the complex energy plane. The wave function in the stub is quenched through the potential barrier; a secondary maximum survives however in between $\tilde{y} = \tilde{l}_2$ and the outermost node at $\tilde{y} = 1$. For strong defect potentials, this trapping of the wave function leads to a long–lived quasi-bound-state, and hence to a very small resonance width. We shall come back

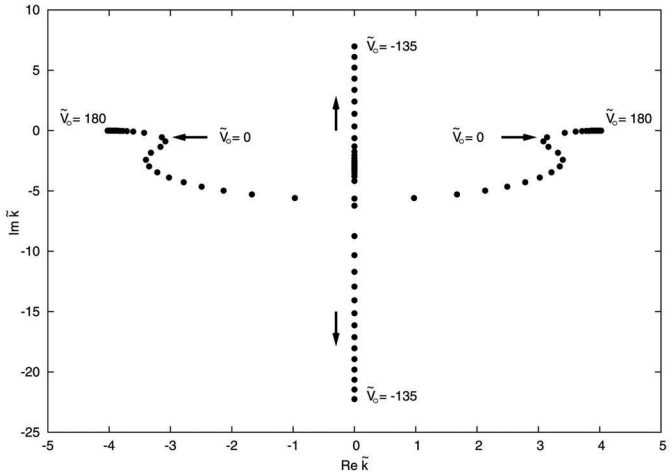

Fig. 2. Trajectory of the $n = 1$ and $n = -1$ poles for $-135 \leq \tilde{V}_0 \leq 180$. The horizontal arrows exhibit the position of the poles for $\tilde{V} = 0$, while the vertical arrows show the motion of the poles on the imaginary axis. The potential and the geometric parameters are the same as in Figure 1.

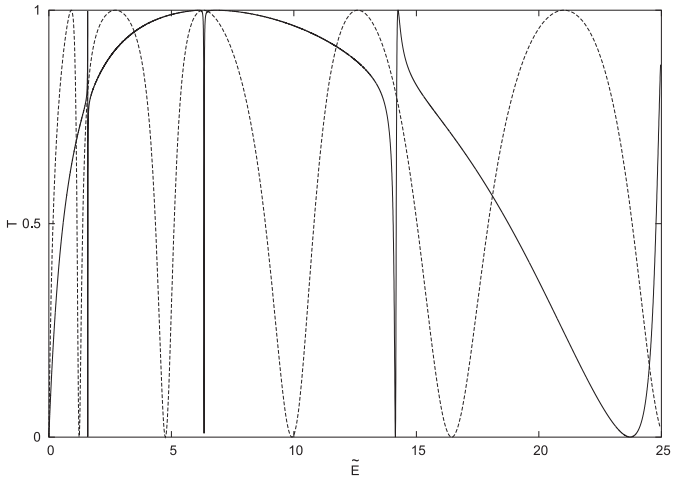

Fig. 3. Transmission coefficient T as a function of the energy $\tilde{E}$ in correspondence to the strength values $\tilde{V}_0 = 5$ (dashed line) and $\tilde{V}_0 = 50$ (solid line). The potential is the same as in Figure 1.

to this point when discussing the dependence of the poles upon the position of the defect in the stub.

For an attractive potential, the two poles move toward the imaginary axis, and coalesce at $\tilde{k} \simeq 0 - 5.64i$, for $\tilde{V}_0 \simeq -22.23$ ($V_0 \simeq -1250$ meV for a stub 100 Å long). As the strength decreases further, one then has two anti-bound-state poles resulting from the "collision", and moving on the imaginary axis in opposite directions. When $\tilde{V}_0 \simeq -101$ the upward moving pole crosses the origin, and emerges in the physical region as a bound state pole. In such circumstances, the potential in the resonator is able to support two bound states, one originating from the zero-order pole, and the new one, coming from the lowest resonance with $n = 1$. We have verified that the poles with $n = \pm 2, \pm 3, \pm 4$ follow similar trajectories, the only difference being that they merge on the imaginary axis at increasing distances from the origin, and for more negative values of the coupling constant. This behavior is strongly reminiscent of what happens for s-wave scattering off an attractive spherical well [15]. There, as the absolute value of the strength increases, the poles move upward in pairs in the unphysical part of the complex k-plane, and approach the imaginary axis, where they overlap, and give rise to poles moving in opposite directions. Differently from the simple potential-scattering case, however, in the present situation one has a sequence of poles at a finite distance from the real axis also when the potential is switched off, because of the coupling of the conducting wire with the resonator.

As stressed in references [13,14], the actual behavior of the device depends upon the position of both the poles and the transmission zeros of the scattering matrix. The motion of the latter along the real, positive axis with varying strength is simple, and reflects what one would expect on physical grounds. For an increasingly attractive potential in the sidearm, the zeros move toward lower energies, until they reach the scattering threshold at $\tilde{E} = 0$; for a repulsive interaction, they are shifted at higher energies. What really matters, as far as the transmission properties of the system are concerned, is the relative distance between the corresponding zeros and poles. As the strength $\tilde{V}_0$ increases, the first three poles approach more and more closely the corresponding zero, whereas the fourth pole moves far away from its associated zero. This fact has striking consequences for the transmission coefficient T of the device, as illustrated in Figure 3, where we plot T as a function of the energy $\tilde{E}$ for $\tilde{V}_0 = 5$ and $\tilde{V}_0 = 50$. In correspondence to the stronger interaction, the "collapse" of the first three zero-pole pairs gives rise to a shrinking of the first three resonance dips, with respect to the weak-interacting case.

As Figure 3 clearly exhibits, the dips in the transmission coefficient are characterized by a more or less pronounced asymmetry. These line shapes are usually parametrized in terms of the Fano function [12,21]

$$T_F = T_0 \frac{(\epsilon + q)^2}{1 + \epsilon^2}, \tag{20}$$

where T_0 is the amplitude of the Fano resonance, $\epsilon \equiv (\tilde{E} - \tilde{E}^{(R)})/\tilde{\Gamma}$ represents the reduced or normalized energy, and we have written the pole location $\tilde{E}^{(p)}$ in the energy plane as $\tilde{E}^{(p)} = \tilde{E}^{(R)} - i\tilde{\Gamma}$. The Fano parameter q is a measure for the ratio between the resonant and non-resonant transmission amplitudes, and determines the asymmetry of the line shape. For one-dimensional systems, there is a simple relation between q and the positions $\tilde{E}^{(R)} - i\tilde{\Gamma}$, $\tilde{E}^{(o)}$ of poles and zeros in the energy plane, namely [13]

$$q = \frac{\tilde{E}^{(R)} - \tilde{E}^{(o)}}{\tilde{\Gamma}}. \tag{21}$$

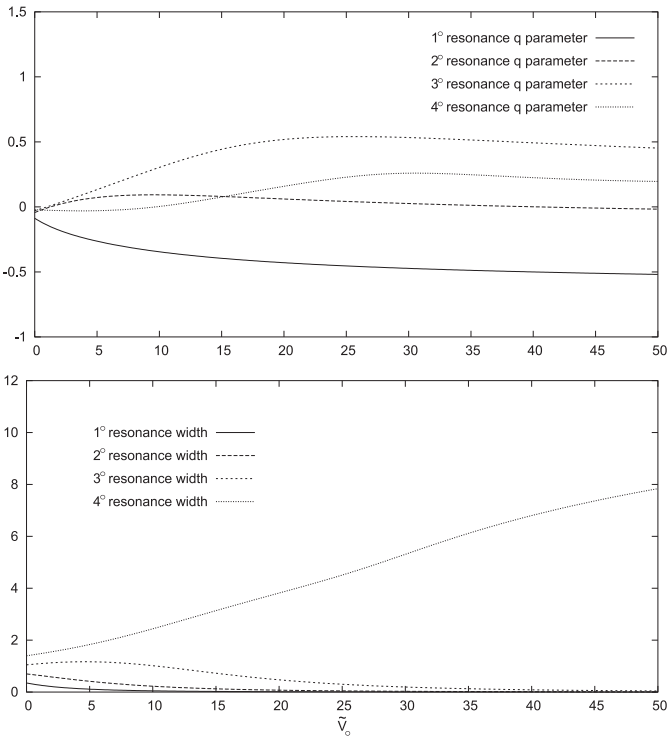

Fig. 4. Fano parameter q (upper panel) and width $\tilde{\Gamma}$ (lower panel) as functions of the adimensional strength $\tilde{V}_0$ for the first four transmission resonances. The potential is the same as in Figure 1.

With reference to Figure 3, for $\tilde{V}_0 = 5$ the Fano parameters of the four resonances one encounters with increasing energy are $q_1 = -0.264$, $q_2 = 0.072$, $q_3 = 0.133$, and $q_4 = -0.029$, respectively, the corresponding widths being $\tilde{\Gamma}_1 = 0.111$, $\tilde{\Gamma}_2 = 0.415$, $\tilde{\Gamma}_3 = 1.167$, and $\tilde{\Gamma}_4 = 1.830$. When the strength $\tilde{V}_0$ is increased up to 50, the widths of the first three resonances reduce to $\tilde{\Gamma}_1 = 0.001$, $\tilde{\Gamma}_2 = 0.007$, and $\tilde{\Gamma}_3 = 0.042$, whereas the width of the fourth, higher-energy resonance has increased up to $\tilde{\Gamma}_4 = 7.843$. As for the Fano parameters, they generally increase in absolute value, their magnitudes being now $q_1 = -0.520$, $q_2 = -0.018$, $q_3 = 0.452$, and $q_4 = 0.196$.

We performed a systematic analysis of the dependence of q upon the strength $\tilde{V}_0$ of the defect. The results of the calculations are given in the upper panel of Figure 4 for the first four resonances.

Apart from a rather limited region, where the asymmetry parameters move away from their initial zero values as the interaction is switched on, one finds a rather mild dependence upon the strength for $\tilde{V}_0 > 20$. This fact can be easily understood in the light of equation (21). When the interaction gets stronger and stronger, the widths of the first three dips vanish, whereas the width of the fourth resonance increases, as the lower panel in Figure 4 exhibits. This strength dependence is to a large extent compensated by a similar change of the zero-pole distances, so that a smooth variation of q with $\tilde{V}_0$ emerges.

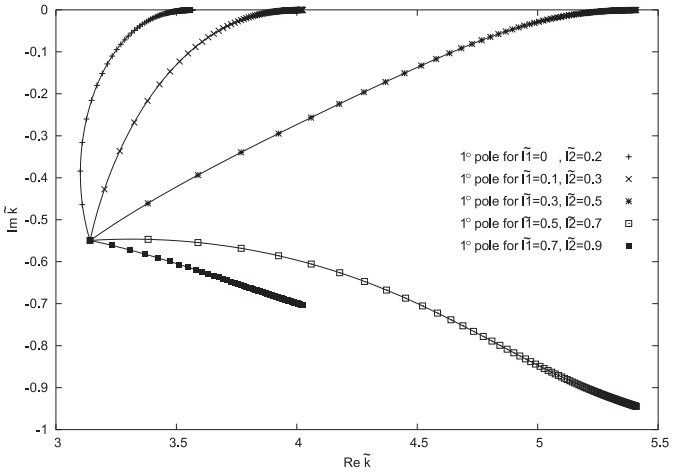

Fig. 5. Trajectories of the $n = 1$ pole in the complex k-plane for different positions of the defect. The pole is plotted in steps $\Delta\tilde{V}_0 = 1$, with $0 \leq \tilde{V}_0 \leq 90$.

Let us finally consider the pole behavior in the complex k-plane, when the position of the defect inside the stub is varied. For an attractive interaction, the scenario is essentially the same as above; in general, the poles in the fourth quadrant and their mirror images in the third move toward the negative imaginary axis, the main difference being that the point where they merge together occurs for increasing values of $\mathrm{Im}\tilde{k}$, i.e., for $n = 1$ the position of the collision point ranges from $\mathrm{Im}\tilde{k} \simeq -5.8$ up to $\mathrm{Im}\tilde{k} \simeq -1.8$, in correspondence to $\tilde{l}_1 = 0.1$, $\tilde{l}_2 = 0.3$, and $\tilde{l}_1 = 0.7$, $\tilde{l}_2 = 0.9$, respectively. Similarly, one finds that the $n = \pm 2$ poles meet at $\mathrm{Im}\tilde{k} \simeq -6.8$, when $\tilde{l}_1 = 0.1$, $\tilde{l}_2 = 0.3$, whereas they collide at $\mathrm{Im}\tilde{k} \simeq -2.1$ for $\tilde{l}_1 = 0.7$, $\tilde{l}_2 = 0.9$. After the collision, one observes again two poles moving in opposite directions on the imaginary axis as the potential gets more and more attractive, until the upward moving pole enters the physical region and a new bound state appears. It is worth to stress that there may be remarkable exceptions to this general trend. For instance, when the attractive potential is placed just on top of the junction point, the first-order ($n = 1$) pole never reaches the imaginary axis; on the contrary, it moves counterclockwise in the fourth quadrant, along a spiraling trajectory, whereas the $n = \pm 2$ poles follow the general trend, meeting each other on the negative imaginary axis, even when $\tilde{l}_1 = 0$.

In correspondence to positive strengths, the pole trajectories are quite sensitive to the defect position inside the resonator. This is illustrated in Figure 5, where we plot the trajectory of the $n = 1$ pole with varying $\tilde{V}_0$, for different values of $\tilde{l}_1$. As the defect is displaced away from the junction, the pole no longer approaches the real axis and, when the defect is contained in the outermost part of the stub, it moves away from the physical region.

The dependence of the pole trajectory upon the position of the potential can be explained through a wave function argument. In Figure 6 we give the square modulus

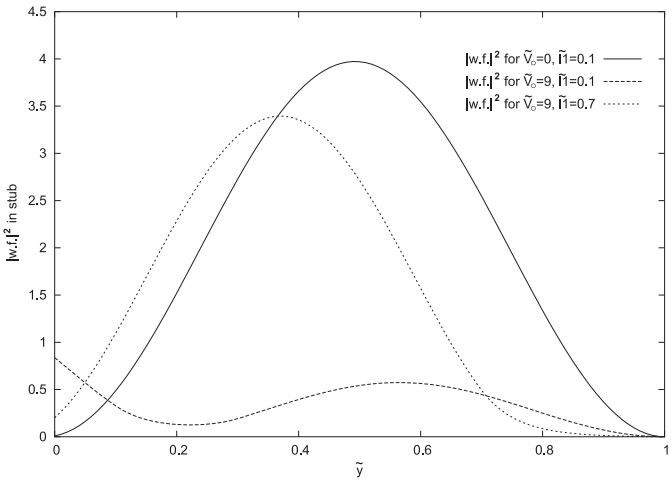

Fig. 6. The square modulus of the stub wave function for the empty stub (full line), and in presence of a potential with $\tilde{V}_0 = 9$, for $\tilde{l}_1 = 0.1$, $\tilde{l}_2 = 0.3$ (dashed line), and $\tilde{l}_1 = 0.7$, $\tilde{l}_2 = 0.9$ (short-dashed line). In all cases the wave function has been evaluated in correspondence to the resonance energy $\mathrm{Re}E_1^{(p)}$.

of the resonant wave function in the stub for $\tilde{V}_0 = 9$, in correspondence with two different positions of the defect, $\tilde{l}_1 = 0.1$ and $\tilde{l}_2 = 0.3$ (dashed line), and $\tilde{l}_1 = 0.7$ and $\tilde{l}_2 = 0.9$ (short-dashed line). For comparison, the resonant wave function for the empty stub is also given (full line). With the repulsive potential switched on, the wave function is quenched in correspondence to the defect region, as we already observed above; when the potential is located near the origin of the stub, the wave function exhibits a maximum in between $\tilde{l}_2$ and the end of the stub, a signal of its trapping inside the resonator; when the potential is centered in the outermost part of the stub, on the other hand, the wave function exhibits only a decreasing tail beyond $\tilde{l}_2$, and the electron is less trapped inside the stub. As a consequence, for the same repulsive strength, one can have a narrow transmission resonance, or a broad structure in the conductivity, depending upon the position of the potential.

Finally, we observe that a quantum circuit quite similar to the device studied in the present paper has been considered in reference [22], to model a quantum connecting wire with a side-coupled quantum dot. In reference [22] the T junction was coupled to a tunable resonator consisting of a tunnel barrier and a perfect reflector. We verified that, displacing in our device the potential to the outermost position in the sidearm, one gets Fano transmission dips all having a negative asymmetry parameter, consistently with reference [22]. Moreover, in this configuration the q parameters turn out to be almost independent upon the strength and the shape (square or smooth) of the potential, an indication that the actual device can be modelled by this simple quantum circuit, without specific assumptions about its features.

4 Conclusions

We have studied the trajectories in the complex momentum plane of the poles of the scattering matrix, for a one-dimensional wire which communicates with a resonator containing a defect potential. We looked at the dependence of the zeros and singularities upon both the strength of the interaction, and its position inside the sidearm. For an attractive interaction, we found a behavior reminiscent of what is found for the standard potential scattering situation; the poles in the fourth and third quadrants move in pairs from the unperturbed positions, and approach the negative imaginary axis, where they merge for a critical value of the strength. As the interaction becomes more and more attractive, one then has two poles moving in opposite directions along the imaginary axis, the upward moving pole entering finally the physical part of the imaginary axis, in correspondence to a new bound state of the system. For repulsive potentials, the resonance pole trajectories depend in a remarkable way upon the position of the defect in the resonator, and can either approach the positive real axis or move away from it in the fourth quadrant. This can be traced back to the trapping or leaking of the electron wave function in the sidearm, a phenomenon which is extremely sensitive to the defect location. The actual shape of the transmission coefficient as a function of the energy depends in principle upon the relative distances of the zero-pole pairs. As far as the Fano asymmetry parameter is concerned, however, there is to some extent a compensation between the zero-pole distances and the corresponding widths $\tilde{\Gamma}$, resulting in an overall mild dependence of q upon $\tilde{V}_0$. Another problem which would deserve a specific analysis is the possible interference among the resonances. That this could actually be the case is signaled by Figure 3, where one observes an increase of the width of the fourth resonance with increasing strength. Energy dependent effects in the overlapping regime can be studied most efficiently through the eigenfunctions of the Hamiltonian of the system, to calculate the coupling matrix elements between system and environment [23]. This kind of analysis, while beyond the scope of the present paper, is presently under consideration.

References

1. S. Datta, *Electronic Transport in Mesoscopic systems* (Cambridge University Press, Cambridge, 1995)
2. D.K. Ferry, M. Goodnick, *Transport in Nanostructures* (Cambridge University Press, Cambridge, 1997)
3. R. Büttiker, Y. Imry, R. Landauer, S. Pinhas, Phys. Rev. B **31**, 6207 (1985)
4. F. Sols, M. Macucci, U. Ravaioli, K. Hess, J. Appl. Phys. **66**, 3892 (1989)
5. H. Wu, D.W.L. Sprung, J. Martorell, S. Klarsfeld, Phys. Rev. B **44**, 6351 (1991)
6. P. Debray, O.E. Raichev, P. Vasilopoulos, M. Rahman, R. Perrin, W.C. Mitchell, Phys. Rev. B **61**, 10950 (2000)
7. X.F. Wang, P. Vasilopoulos, F.M. Peeters, Phys. Rev. B **65**, 165217 (2002)

8. S. Rotter, J.-Z. Tang, L. Wirtz, J. Trost, J. Burgdörfer, Phys. Rev. B **62**, 1950 (2000)
9. S. Rotter, B.W. Weingartner, N. Rohringer, J. Burgdörfer, Phys. Rev. B **68**, 165302 (2003)
10. B.W. Weingartner, S. Rotter, J. Burgdörfer, Phys. Rev. B **72**, 115342 (2005)
11. D.Y.K. Ko, J.C. Inkson, Phys. Rev. B **38**, 9945 (1988)
12. J.U. Nöckel, A.D. Stone, Phys. Rev. B **50**, 17415 (1994)
13. W. Porod, Z. Shao, C.S. Lent, Phys. Rev. B **48**, 8495 (1993)
14. Z. Shao, W. Porod, C.S. Lent, Phys. Rev. B **49**, 7453 (1994)
15. H.M. Nussenzveig, Nucl. Phys. **11**, 499 (1959)
16. H.M. Nussenzveig, *Causality and dispersion relations* (Academic Press, New York, 1972)
17. R.G. Newton, *Scattering Theory of Waves and Particles* (Springer, New York, 1982), pp. 331–401
18. J.E. Avron, A. Raveh, B. Zur, Rev. Mod. Phys. **60**, 873 (1988)
19. F. Dittes, Phys. Rep. **339**, 215 (2000)
20. W.-D. Sheng, J.-B. Xia, J. Phys.: Condens. Matter **8**, 3635 (1996)
21. U. Fano, Phys. Rev. **124**, 1866 (1961)
22. K. Kobayashi, H. Aikawa, A. Sano, S. Katsumoto, Y. Iye, Phys. Rev. B **70**, 035319 (2004)
23. J. Okołowicz, M. Płoszajczak, I. Rotter, Phys. Rep. **374**, 271 (2003)